JOURNAL OF SYNCHROTRON RADIATION

ISSN 1600-5775

Helicity-dependent resonant X-ray scattering in CuB_2O_4

E. N. Ovchinnikova,[a]* A. Rogalev,[b] F. Wilhelm,[b] F. de Bergevin,[b] V. E. Dmitrienko,[c] A. P. Oreshko,[a] K. A. Kozlovskaya[a]* and R. D. Bakonin[a]

[a]Physics Department, Moscow State University, Moscow 119899, Russia, [b]European Synchrotron Radiation Facility, 38000 Grenoble, France, and [c]A. V. Shubnikov Institute of Crystallography, FSRC Crystallography and Photonics RAS, Moscow 119333, Russia. *Correspondence e-mail: en_ovchinnikova@physics.msu.ru, kozlovskaya@physics.msu.ru

Received 26 April 2021
Accepted 6 June 2021

Edited by A. Stevenson, Australian Synchrotron, Australia

Keywords: X-ray absorption; X-ray natural circular dichroism; resonant X-ray scattering.

Exploitation of X-ray circular polarized beams to study forbidden Bragg reflections and new information that could be obtained in these experiments are discussed. It is shown that the intensities of such reflections can be different for the right- and left-circular polarizations (*i.e.* exhibiting circular dichroism) even for the dipole–dipole resonant transitions involved in the scattering process. This difference can be observed only in crystals having no center of inversion. Here, this approach is used to study helicity-dependent resonant diffraction in copper metaborate CuB_2O_4 single crystal, which is non-centrosymmetric but achiral. Nonetheless, a strong circular dichroism has been observed for *hh*0 forbidden reflections in the vicinity of the Cu *K*-edge. This effect is shown to originate from dipolar transitions in Cu atoms occupying the 8(*d*) Wyckoff position only.

1. Introduction

The physical properties of a solid and its crystal structure are closely related and understanding this relationship is one of the greatest challenges of material science, especially in view of engineering materials with new functionalities. Materials with no inversion symmetry attract special attention because they could exhibit intriguing physical properties like multiferroicity and piezoelectricity. Chirality of matter (the existence of the right- and left-handed forms) is believed to be an internal property determined by atomic arrangement featuring no inversion center. This property plays a crucial role in biology and pharmaceutics but is also very important in physical phenomena and technological applications. Thanks to the development of X-ray spectroscopy at third-generation synchrotrons, it became possible to probe chirality on a microscopic level using X-ray natural circular dichroism (XNCD) (Alagna *et al.*, 1998; Goulon *et al.*, 1998, 1999, 2003; Natoli *et al.*, 1998; Carra & Benoist, 2000; Peacock & Stewart, 2001; Izumi *et al.*, 2013; Platunov *et al.*, 2021). XNCD occurs at photon energies close to an absorption edge due to the electric-dipole–electric-quadrupole *E*1.*E*2 interference terms in absorption cross-section whereas electric-dipole–magnetic-dipole *E*1.*M*1 interference terms, which dominate optical activity in visible optics (Buckingham, 1967; Barron, 1982), become vanishingly small in X-ray spectroscopy. Owing to its *E*1.*E*2 origin, the main drawback of XNCD is that it is observable only in single crystals that belong to 13 out of 21 noncentrosymmetric crystal classes (Jerphagnon & Chemla, 1976; Jerphagnon *et al.*, 1978; Goulon *et al.*, 1998, 1999, 2003). However, XNCD can be applied to opaque samples, whereas

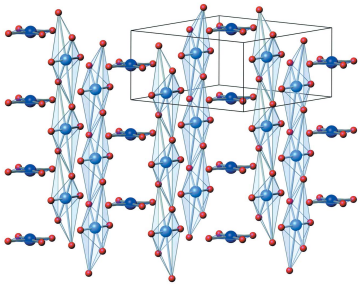

in the visible spectral range circular dichroism can be measured only in transparent substances.

Complementary to X-ray spectroscopy measurements, resonant X-ray scattering (RXS) techniques offer site selectivity to study properties of crystals, among them local symmetry (Belyakov & Dmitrienko, 1989; Dmitrienko & Ovchinnikova, 2003; Dmitrienko *et al.*, 2005; Collins *et al.*, 2007; Lovesey & Collins, 1996), thermal displacements (Dmitrienko *et al.*, 1999; Dmitrienko & Ovchinnikova, 2000; Kokubun *et al.*, 2001; Kirfel *et al.*, 2002; Collins *et al.*, 2003) and local chirality of scattering atoms (Dmitrienko & Ovchinnikova, 2001; Di Matteo *et al.*, 2003). This is because RXS is sensitive to phase shifts of the waves scattered by different atoms in a unit cell as well as to multipole contributions to atomic scattering factors. Unique information related to local chirality can be further obtained from resonant X-ray diffraction using circularly polarized photons. Unfortunately, use of this technique is very scarce.

On the contrary, linear dichroism of Bragg reflections, *i.e.* the difference of their intensities for σ and π polarization of incident radiation, is well known, because it exists even in conventional nonresonant X-ray scattering (James, 1950). In a resonant regime σ and π polarizations can be mixed, leading to a change of polarization during the scattering process. This effect was observed many times in RXS experiments, especially in studies of so-called forbidden reflections. Those are absent when the atomic scattering amplitudes are added in antiphase, *i.e.* the contribution from Thomson scattering vanishes. However, when the photon energies are in the vicinity of an absorption edge (in resonance with transitions from a core state) in a crystal belonging to a non-symmorphic space group, the forbidden reflections could become allowed. Since forbidden reflections result from an anisotropy of electron density of scattering atoms, they appear to be highly sensitive to the local symmetry (Dmitrienko, 1983, 1984; Dmitrienko *et al.*, 2005; Templeton & Templeton, 1985*a*,*b*, 1986).

The resonant X-ray scattering arises from multipole electronic transitions (Blume, 1994; Dmitrienko & Ovchinnikova, 2003; Dmitrienko *et al.*, 2005; Lovesey & Collins, 1996; Lovesey *et al.*, 2005; Collins *et al.*, 2007) and is usually described in terms of scattering tensors of various ranks (Blume, 1994; Hannon *et al.*, 1988). The strongest contribution to forbidden reflections is due to the dipole–dipole $E1.E1$ scattering whereas higher-order contributions, such as dipole–quadrupole $E1.E2$ (Templeton & Templeton, 1994; Dmitrienko & Ovchinnikova, 2001; Di Matteo *et al.*, 2003) or quadruple–quadrupole $E2.E2$ (Carra & Thole, 1994; Finkelstein *et al.*, 1992, 1994), become detectable when the former is weak or absent for symmetry reasons. Interestingly, forbidden reflections that originate from interference between different scattering channels (*e.g.* $E1.E1$ with $E1.E2$) have been experimentally observed (Kirfel *et al.*, 2002; Collins *et al.*, 2003; Beutier *et al.*, 2014, 2015; Richter *et al.*, 2014; Kokubun *et al.*, 2001; Oreshko *et al.*, 2012). However, local chirality could not be fully investigated in these experiments since linearly polarized X-rays were used. In particular, interference with magnetic scattering allows the sign of the Dzyaloshinskii-Moria interaction in canted antiferromagnets to be related to local crystal chirality (Dmitrienko *et al.*, 2010, 2014).

To gain a deeper insight into the local chirality of a crystal, use of circularly polarized X-rays in resonant diffraction experiments is mandatory. For the first time, the 'chirality' of forbidden reflections in RXS was predicted by Dmitrienko (1983). It was shown that the intensities of forbidden reflections in certain chiral symmetries are different for the right- and left-circular polarized X-rays. This was confirmed experimentally for SiO_2 and Te (Tanaka *et al.*, 2008, 2010), in which the 3_1 or 3_2 screw axes give rise to the right-handed or left-handed crystals. Recently the difference between the integrated intensities of the forbidden reflections measured with right- and left-circular polarization was used for the chiral domains imaging in $DyFe_3(BO_3)_4$ (Usui *et al.*, 2014). There was another RXS experiment using circularly polarized radiation that deserves to be mentioned. It concerns observation of the vector part of optical activity in ZnO (Goulon *et al.*, 2007), which crystallizes in the space group $P6_3mc$. Even though this space group is achiral, the difference in the intensity of the allowed 300 Bragg reflection for the right- and left-circularly polarized beams was observed at energies close to the Zn K-edge. It was suggested that this peculiar signal is proportional to an electric dipole moment of the scattering atomic sites (Carra *et al.*, 2003). This experiment has shown the possibility to separate resonant from Thomson scattering in a study of allowed reflections without analyzing the polarization of scattered X-rays, as was recently proposed by Ovchinnikova *et al.* (2019). It is especially important taking into account that many functional materials are described by symmorphic space groups, in which there are no forbidden Bragg reflections.

In this paper, we present a thorough experimental and theoretical study of circular dichroism in forbidden reflections in copper metaborate (CuB_2O_4) single crystal. This crystal recently attracted a lot of attention because of its unique physical properties, like complex magnetic structure with a series of commensurate/incommensurate phase transitions at low temperatures of 21 K, 10 K and 2 K (Boehm *et al.*, 2003), magnetoelectric properties (Khanh *et al.*, 2013; Nénert *et al.*, 2007; Mero *et al.*, 2021), the gigantic optical magnetoelectric effect (Saito *et al.*, 2008*a*), and magnetic-induced second harmonic generation (Pisarev *et al.*, 2004). Moreover, Saito *et al.* (Saito *et al.*, 2008*b*; Arima & Saito; 2009) claimed that it would be possible 'to control the crystal chirality by magnetic field' in copper metaborate. This statement violates the fundamental symmetry principle [see, for example, Lovesey & Staub (2009)] and it was shown that the observed effect can be explained by sublattice-sensitive antiferromagnetic linear dichroism (Boldyrev *et al.*, 2015). Copper metaborate crystallizes in space group $I\bar{4}2d$ which is non-enantiomorphous (right-handed and left-handed crystals do not exist), because its unit cell contains left-handed and right-handed screws, formed by two non-equivalent Cu atoms (Figure 1). The electronic and magnetic properties of these two distinct Cu atoms need to be studied separately. Recently the neutron diffraction and circular dichroism in magnetically ordered

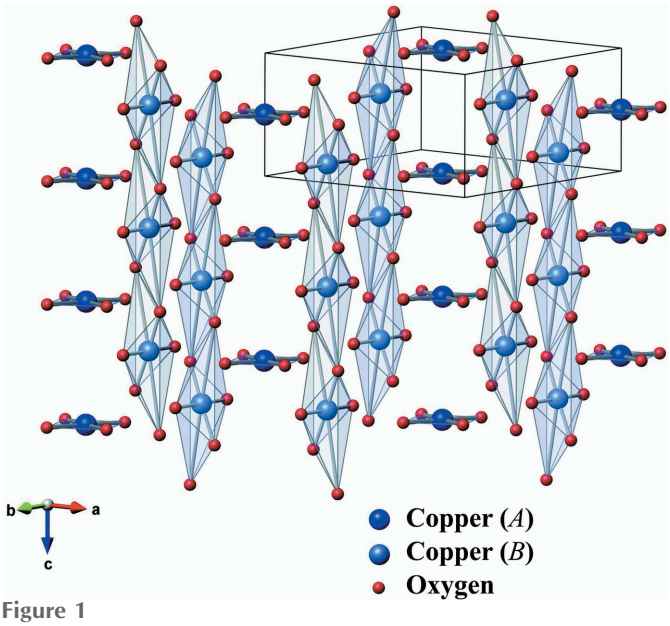

Figure 1
Crystallographic structure of a CuB_2O_4 crystal viewed along a direction close to ⟨110⟩. Boron atoms are not shown.

copper metaborate was considered by Lovesey (2016) within a minimal model of copper atomic sites. The Cu *K*-edge XNCD signal was also measured on this crystal (Ovchinnikova *et al.*, 2016) but all Cu atoms in the unit cell were contributing to it. Circular dichroism in resonant X-ray diffraction offers a unique possibility to perform element- and site-selective study of the electronic properties of crystals. The main goal of the present work is to show that the local electronic structure of one of the two non-equivalent Cu sites in a CuB_2O_4 single crystal can be investigated using circular dichroism in 'forbidden' ⟨*hh*0⟩ reflections at the Cu *K*-edge.

2. Symmetry analysis of resonant X-ray scattering

Whenever the energy of X-rays is close to an absorption edge of an atom, resonant X-ray scattering becomes anisotropic. Indeed, various multipolar transitions between an inner shell and the crystal-field-split excited multiplets of a resonant atom contribute to the atomic scattering factor, which is a tensor. The dipole–dipole contribution to the atomic scattering factor in nonmagnetic crystals is described by a rank-2 tensor whose structure is fully determined by the symmetry of the atomic site. If resonant atoms are in the general Wyckoff position, the dipole–dipole tensor f_{ij}^{s} corresponding to the *s*-atom contains nine elements out of which only six are non-equivalent since $f_{ij} = f_{ji}$. But if resonant atoms are in a special Wyckoff position, its symmetry restricts the number of independent elements since some of them turn out to be zero.

To identify these elements one can use the invariance of the atomic tensor factor under the symmetry operations for a given Wyckoff position (Hahn, 1996),

$$\hat{f}^{s} = R(\hat{h})\,\hat{f}^{s}\,R^{-1}(\hat{h}), \tag{1}$$

where $\hat{h}$ is a symmetry operation of a subgroup of the point group of the crystal.

The structure factor is the sum of atomic scattering factors of all atoms in a unit cell taking into account the rotation of the tensor axes under the symmetry elements of the space group $\hat{g}_s = (\hat{R}_s|\tau_s)$,

$$\hat{F}(\mathbf{H}) = \sum_{s} \hat{R}_s\,\hat{f}^{1}\,\hat{R}_s^{-1}\exp\left[2\pi i\mathbf{H}\left(\hat{R}_s\,\mathbf{r}_1 + \boldsymbol{\tau}_s\right)\right], \tag{2}$$

where $\hat{R}_s$ is the rotational part of the symmetry operation, $\boldsymbol{\tau}_s$ is the corresponding fractional translation, and $\hat{f}^{1}$ is the atomic scattering factor tensor of the atom with coordinates $\mathbf{r}_1$ within a Wyckoff position (Dmitrienko *et al.*, 2013).

The scattering amplitude is obtained through the three-dimensional tensor $\hat{F}$ taken between polarization vectors of the incident α and scattered β radiation. Since those are actually two-dimensional vectors, $\hat{F}$ is commonly represented by 2×2 matrices[1],

$$F_{\beta\alpha} = \epsilon_{\beta}^{*}\,\hat{F}\,\epsilon_{\alpha}. \tag{3}$$

If the polarizations are linear we have in the basis σ, π,

$$(F_{\beta\alpha}) = \begin{pmatrix} F_{\sigma\sigma} & F_{\sigma\pi} \\ F_{\pi\sigma} & F_{\pi\pi} \end{pmatrix}. \tag{4}$$

The nondiagonal terms in (4) may be non-zero in resonant scattering, contrary to the Thomson scattering case. Let us determine the circular polarization vectors as $\mathbf{e}_{+} = (\mathbf{e}_{\pi} + i\mathbf{e}_{\sigma})/\sqrt{2}$, $\mathbf{e}_{+} = (\mathbf{e}_{\pi} - i\mathbf{e}_{\sigma})/\sqrt{2}$. The change of the basis from linear as $(F_{l'l})$, to circular as $(F_{c'c})$, is obtained through

$$(F_{c'c}) = \hat{U}(F_{l'l})\,\hat{U}^{-1}, \tag{5}$$

where $\hat{U}$ and $\hat{U}^{-1}$ are unitary matrices

$$\hat{U} = \frac{1}{\sqrt{2}}\begin{pmatrix} i & 1 \\ -i & 1 \end{pmatrix}, \qquad \hat{U}^{-1} = \frac{1}{\sqrt{2}}\begin{pmatrix} -i & i \\ 1 & 1 \end{pmatrix}. \tag{6}$$

One can express then the scattering amplitude components for circularly + (right) and − (left) polarized radiation,

$$\begin{aligned} 2F_{++} &= F_{\sigma\sigma} + F_{\pi\pi} + i\left(F_{\sigma\pi} - F_{\pi\sigma}\right), \\ 2F_{+-} &= -F_{\sigma\sigma} + F_{\pi\pi} + i\left(F_{\sigma\pi} + F_{\pi\sigma}\right), \\ 2F_{-+} &= -F_{\sigma\sigma} + F_{\pi\pi} - i\left(F_{\sigma\pi} + F_{\pi\sigma}\right), \\ 2F_{--} &= F_{\sigma\sigma} + F_{\pi\pi} - i\left(F_{\sigma\pi} - F_{\pi\sigma}\right). \end{aligned} \tag{7}$$

The intensity of the diffracted radiation is a function of photon energy and proportional to

$$I_{\beta\alpha}(\mathbf{H}, \hbar\omega) \;\propto\; \left|\epsilon_{\beta}^{*}\,F_{\beta\alpha}(\mathbf{H}, \hbar\omega)\,\epsilon_{\alpha}\right|^{2}/\mu_{\alpha}(\hbar\omega). \tag{8}$$

This formulation is valid in kinematic diffraction theory for an infinitely thick sample with **H** perpendicular to the sample surface. The absorption coefficient $\mu_{\alpha}(\hbar\omega)$ can be represented as a sum of the nonresonant, dipole and quadrupole terms (Brouder, 1990). Even though linear and circular dichroisms have been measured at the Cu *K*-edge spectra in copper metaborate crystal (Ovchinnikova *et al.*, 2016), they are rather

[1] In this representation the matrix $(F_{\alpha\beta})$ is no longer symmetric.

weak and we therefore neglect the polarization dependence of absorption, *i.e.* we use the isotropic spectrum $\mu(\hbar\omega)$.

At energies close to an absorption edge the anisotropy of resonant scattering removes some extinctions of Bragg reflections corresponding to the screw axes and glide planes, even in the dipole–dipole approximation (Dmitrienko, 1983, 1984). Polarization properties of these reflections were also considered by Belyakov & Dmitrienko (1989) and the intensities of some of them were shown to be different for incident right- and left-circularly polarized radiation, *i.e.* they exhibit 'circular dichroism'. We would like to underline that this 'circular dichroism' is fundamentally different from circular dichroism in absorption and in diffraction for allowed reflections (Goulon *et al.*, 2007). The latter is observable only when the electronic states with mixed parity are excited *via* the $E1.E2$ resonant channel. The circular dichroism in the diffraction experiment could be expressed in the following manner,

$$\Delta I(hkl) = I_+ - I_- = |F_{++}|^2 + |F_{-+}|^2 - |F_{+-}|^2 - |F_{--}|^2. \tag{9}$$

We can also rewrite (9) in linear polarizations basis,

$$\begin{aligned}\Delta I(hkl) &= I_+ - I_- \\ &= 2\left[F'_{\pi\pi}F''_{\pi\sigma} - F''_{\pi\pi}F'_{\pi\sigma} + F''_{\sigma\sigma}F'_{\sigma\pi} - F'_{\sigma\sigma}F''_{\sigma\pi}\right],\end{aligned} \tag{10}$$

where F' and F'' are the real and imaginary parts of the complex scattering amplitudes. One can see from (10) that the necessary condition for circular dichroism in Bragg diffraction is the intermixing of σ and π polarizations in the scattering process. Indeed, this circular dichroism of a non-magnetic reflection is absent in the $E1.E1$ approximation when a crystal has a center of inversion. The atomic scattering factor, considered to be non-magnetic, is invariant in the $E1.E1$ approximation under the space inversion; the incident and diffracted X-ray wavevectors as well as the atomic positions are unchanged whereas the circular polarization is reversed, so that the diffracted intensities for right- and left-circularly polarized X-rays should be strictly identical.

Given the fact that copper metaborate crystal has no inversion center, one could therefore observe circular dichroism in Bragg diffraction even in the $E1.E1$ approximation. Below we consider circular dichroism of $\langle hh0\rangle$ 'forbidden' reflections in copper metaborate crystal.

2.1. Circular dichroism of the forbidden reflections in copper metaborate: dipole–dipole scattering

At room temperature, CuB_2O_4 crystallizes in the tetragonal noncentrosymmetric space group $I\bar{4}2d$ (No. 122) (Martinez-Ripoll *et al.*, 1971) with 12 formula units in a cell of dimensions $a = 11.484$ Å and $c = 5.620$ Å. The unit cell is shown in Figure 1. There are two non-equivalent sites occupied by Cu^{2+} ions. The Cu^{2+} ions in 4(b) Wyckoff positions (A-sites with coordinates $(0, 0, 1/2)$ and $(1/2, 0, 1/4)$) are surrounded by four oxygen atoms in planar quadratic coordination so that the local symmetry is $\bar{4}$. The Cu^{2+} ions in the 8(d) Wyckoff positions [B-sites with coordinates $(x, 1/4, 1/8)$, $(\bar{x}, 3/4, 1/8)$, $(1/4, \bar{x}, 7/8)$, $(3/4, x, 7/8)$ where $x = 0.0815$] are located in the center of a distorted octahedron with an exceptionally large distance of 3.069 Å to the two apical oxygen ions. As a consequence the local symmetry of this site is 2.

The presence of two substantially different copper sublattices leads to a number of interesting and unusual optical and magnetic properties. Despite the fact that both Cu ions have the same Cu^{2+} electronic configuration, only the Cu(A) sublattice spontaneously orders at the Neel temperature T_N = 21 K into an antiferromagnetic commensurate structure with magnetic moments lying in the (ab)-plane. These moments are slightly canted due to the Dzyaloshinskii-Moriya interaction yielding a weak ferromagnetic moment along the [110] direction (Petrakovskii *et al.*, 1999). Whereas the Cu(A) magnetic moments reach the value $0.86\,\mu_B$ at 12 K, the Cu(B) ions acquire a magnetic moment of only $0.2\,\mu_B$ at the same temperature. Below the phase transition into an incommensurate helicoidal phase at 10 K, this moment starts to increase, reaching $0.54\,\mu_B$ at 2 K. The Cu(B) sublattice is not fully ordered and the moments fluctuate even at the lowest temperature. The precise determination of its magnetic behavior is consequently very difficult (Boehm *et al.*, 2003; Nénert *et al.*, 2007; Fiebig *et al.*, 2003). To obtain a deeper insight into the electronic structure of the Cu(B) site only is highly desirable. As we show below, the resonant X-ray diffraction using forbidden $hh0$ reflections allows us to obtain this information.

Using equation (1) and given the site symmetry $\bar{4}$ of the Cu(A) site, the corresponding atomic scattering tensor in the dipole–dipole approximation has only two non-equivalent components: $f_{xx}(A)$ and $f_{zz}(A)$. The symmetry of the unit cell imposes that

$$f_{ij}(A1) = f_{ij}(A2) = \begin{pmatrix} f_{xx}(A) & 0 & 0 \\ 0 & f_{xx}(A) & 0 \\ 0 & 0 & f_{zz}(A) \end{pmatrix}, \tag{11}$$

where $f_{ij}(An)$ describes the scattering factors of copper atoms occupying A-sites. For the 4(b) Wyckoff position, $n = 1, 2, 3, 4$, but translation $(1/2, 1/2, 1/2)$ does not change $f_{ij}(An)$, therefore there are only two different scattering factors corresponding to Cu(A) sites. Coefficients f_{ij} are complex values and in the dipole–dipole approximation can be calculated by the following,

$$f'_{ij} + if''_{ij} = \frac{m}{\hbar^3\omega}\sum_{f,g}\left(E_f - E_g\right)^3 \frac{D_{ij}}{\hbar\omega - \left(E_f - E_g\right) - i\Gamma/2\hbar}, \tag{12}$$

$$D_{ij} = \left\langle g\left|R_i\right|f\right\rangle\left\langle f\left|R_j\right|g\right\rangle, \tag{13}$$

where $\mathbf{R} = \sum_s \mathbf{r}^s$ is a sum over all electrons in the atom, E_g and E_f are the energies of the ground and excited states, and Γ is the width of the excited state, also depending on E.

The site symmetry 2 of the Cu(B) site implies that there are only four independent components (see Sirotine & Chaskolskaia, 1982); the symmetry operations of the crystal

allows us to express the corresponding atomic scattering tensor as

$$f_{ij}(B1) = \begin{pmatrix} f_{xx}(B) & 0 & 0 \\ 0 & f_{yy}(B) & f_{yz}(B) \\ 0 & f_{yz}(B) & f_{zz}(B) \end{pmatrix}, \quad (14)$$

$$f_{ij}(B2) = \begin{pmatrix} f_{xx}(B) & 0 & 0 \\ 0 & f_{yy}(B) & -f_{yz}(B) \\ 0 & -f_{yz}(B) & f_{zz}(B) \end{pmatrix}, \quad (15)$$

$$f_{ij}(B3) = \begin{pmatrix} f_{yy}(B) & 0 & -f_{yz}(B) \\ 0 & f_{xx}(B) & 0 \\ -f_{yz}(B) & 0 & f_{zz}(B) \end{pmatrix}, \quad (16)$$

$$f_{ij}(B4) = \begin{pmatrix} f_{yy}(B) & 0 & f_{yz}(B) \\ 0 & f_{yy}(B) & 0 \\ f_{yz}(B) & 0 & f_{zz}(B) \end{pmatrix}, \quad (17)$$

where $f_{ij}(Bn)$ corresponds to the copper atoms of B-sites. For the B-position, $n = 1, \ldots, 8$. However, there are only four different scattering factors $f_{ij}(Bn)$, because translation (1/2, 1/2, 1/2) does not change their value. Let us note that components $f_{ij}(An)$ and $f_{ij}(Bn)$ are energy-dependent and complex.

In the space group $I\bar{4}2d$ of copper metaborate the reflections hhl, $2h + l = 4n + 2$, are forbidden off resonance due to a glide-plane symmetry (Hahn, 1996). In the particular case of $hh0$, $h = 2n + 1$, the Cartesian components of the scattering tensor $\hat{F}$ defined in equation (2) are given by

$$\begin{aligned} F_{ij}(hh0, h = 2n+1) = {} & 2\big[f_{ij}(A1) - f_{ij}(A2)\big] \\ & + 2i\big\{\exp(2\pi i h x)\big[f_{ij}(B4) - f_{ij}(B1)\big] \\ & + \exp(-2\pi i h x)\big[f_{ij}(B2) - f_{ij}(B3)\big]\big\}. \end{aligned} \quad (18)$$

The factor of two in equation (18) takes into account the fact that there are only two different atomic factors for copper atoms in Wyckoff position 4(b) and four atomic factors in the position 8(d). Taking into account that $f_{ij}(A1) = f_{ij}(A2)$ [see (11)], the contribution of the Cu(A) atoms is canceled and only copper atoms occupying B sites contribute to the $hh0$ dipole–dipole resonant X-ray scattering near the Cu K-edge. In fact, Cu(A) atoms can contribute to this forbidden reflection but only in the dipole–quadrupole approximation, which is much weaker and, therefore, neglected here. Finally, the structure factor tensor for the $hh0$ ($h = 2n + 1$) reflections in the dipole–dipole approximation for the CuB_2O_4 crystal takes the following form,

$$F(hh0, h = 2n+1) \simeq 4(-1)^{n+1} \times \begin{pmatrix} [f_{xx}(B) - f_{yy}(B)]\sin 2\pi h x & 0 & i f_{yz}(B)\cos 2\pi h x \\ 0 & -[f_{xx}(B) - f_{yy}(B)]\sin 2\pi h x & -i f_{yz}(B)\cos 2\pi h x \\ i f_{yz}(B)\cos 2\pi h x & -i f_{yz}(B)\cos 2\pi h x & 0 \end{pmatrix}. \quad (19)$$

Let us now calculate the circular dichroism for $hh0$ ($h = 2n + 1$) forbidden reflections and its azimuthal dependence. The corresponding diffraction geometry is shown in Figure 2. The

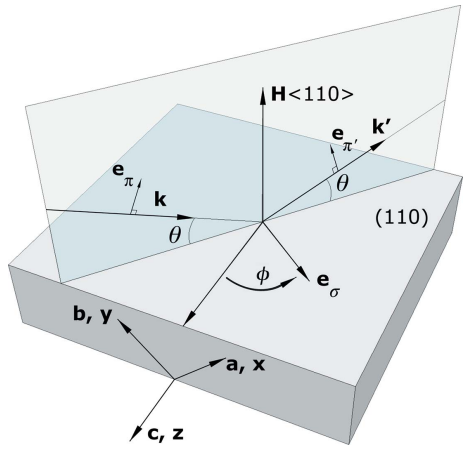

Figure 2
Geometry of the diffraction experiment.

lattice vectors define the reference frame. The incident and diffracted wavevectors are then given by

$$\begin{aligned} \mathbf{k} &= \begin{pmatrix} -(\sqrt{2}/2)(\sin\theta - \cos\theta\cos\phi) \\ -(\sqrt{2}/2)(\sin\theta + \cos\theta\cos\phi) \\ -\cos\theta\sin\phi \end{pmatrix}, \\ \mathbf{k}' &= \begin{pmatrix} (\sqrt{2}/2)(\sin\theta + \cos\theta\cos\phi) \\ (\sqrt{2}/2)(\sin\theta - \cos\theta\cos\phi) \\ -\cos\theta\sin\phi \end{pmatrix}, \end{aligned} \quad (20)$$

where θ is the Bragg angle and ϕ is an angle around the scattering vector. The corresponding polarization vectors are

$$\begin{aligned} \mathbf{e}_\sigma &= \begin{pmatrix} (\sqrt{2}/2)\sin\phi \\ -(\sqrt{2}/2)\sin\phi \\ \cos\phi \end{pmatrix}, \\ \mathbf{e}_\pi &= \begin{pmatrix} -(\sqrt{2}/2)(\cos\phi\sin\theta + \cos\theta) \\ (\sqrt{2}/2)(\cos\phi\sin\theta - \cos\theta) \\ \sin\theta\sin\phi \end{pmatrix} \end{aligned} \quad (21)$$

and

$$\begin{aligned} \mathbf{e}'_\sigma &= \begin{pmatrix} (\sqrt{2}/2)\sin\phi \\ -(\sqrt{2}/2)\sin\phi \\ \cos\phi \end{pmatrix}, \\ \mathbf{e}'_\pi &= \begin{pmatrix} (\sqrt{2}/2)(\cos\phi\sin\theta - \cos\theta) \\ -(\sqrt{2}/2)(\cos\phi\sin\theta + \cos\theta) \\ -\sin\theta\sin\phi \end{pmatrix}. \end{aligned} \quad (22)$$

Both wavevectors $\mathbf{k}$, $\mathbf{k}'$ and polarization vectors $\mathbf{e}_\pi$, $\mathbf{e}'_\pi$, $\mathbf{e}_\sigma$, $\mathbf{e}'_\sigma$ are unit vectors.

Using equations (3) and (19) the components of the scattering amplitude tensor in linear polarization basis are expressed as follows,

$$F_{\sigma\sigma} = \sqrt{2}\, i f_{yz} \sin 2\phi \cos(2\pi h x), \quad (23)$$

$$F_{\sigma\pi} = -\left(f_{xx} - f_{yy}\right)\sin\phi\cos\theta\sin(2\pi hx) - \sqrt{2}\,if_{yz}\cos 2\phi\sin\theta\cos(2\pi hx), \quad (24)$$

$$F_{\pi\sigma} = -\left(f_{xx} - f_{yy}\right)\sin\phi\cos\theta\sin(2\pi hx) + \sqrt{2}\,if_{yz}\cos 2\phi\sin\theta\cos(2\pi hx), \quad (25)$$

$$F_{\pi\pi} = \sqrt{2}\,if_{yz}\sin 2\phi\sin^2\theta\cos(2\pi hx). \quad (26)$$

The polarization-averaged intensity of the $hh0$ reflections is then given by

$$\begin{aligned} I(hh0)_{\rm av} &= I(hh0)_+ - I(hh0)_- \\ &= |F_{++}|^2 + |F_{-+}|^2 + |F_{+-}|^2 + |F_{--}|^2 \\ &= |F_{\sigma\sigma}|^2 + |F_{\sigma\pi}|^2 + |F_{\pi\sigma}|^2 + |F_{\pi\pi}|^2 \\ &= |f_{yz}|^2\left[(1+\sin^4\theta)\sin^2(2\phi) + 2\sin^2\theta\cos^2(2\phi)\right]\cos^2(2\pi hx) \\ &\quad + |f_{xx} - f_{yy}|^2\sin^2\phi\cos^2\theta\sin^2(2\pi hx). \end{aligned} \quad (27)$$

Inserting the components of the scattering amplitude tensor into equation (10) we find that the circular dichroism of the forbidden $hh0$ reflection in the dipole–dipole approximation is equal to

$$\begin{aligned} \Delta I_\pm(hh0) &= I(hh0)_+ - I(hh0)_- \\ &= \sqrt{2}\sin\phi\sin(2\phi)\cos^3\theta\sin(4\pi hx) \\ &\quad \times \left[{\rm Re}\left(f_{yz}\right){\rm Re}\left(f_{xx} - f_{yy}\right) + {\rm Im}\left(f_{yz}\right){\rm Im}\left(f_{xx} - f_{yy}\right)\right], \end{aligned} \quad (28)$$

where ${\rm Re}(f)$ and ${\rm Im}(f)$ are the real and imaginary parts of the atomic tensor factor. We can see from (28) that the dichroism $\Delta I_\pm(hh0)$ has the same azimuthal dependence for all $hh0$ reflections (see Figure 3) and only its amplitude is varying with h. The values of the $\sin(4\pi hx)$ and of the Bragg angle for incident photon energies of 8.99 keV and for different $hh0$ reflections as well as the relative amplitudes of circular dichroism with respect to that of the 110 reflection are given in Table 1.

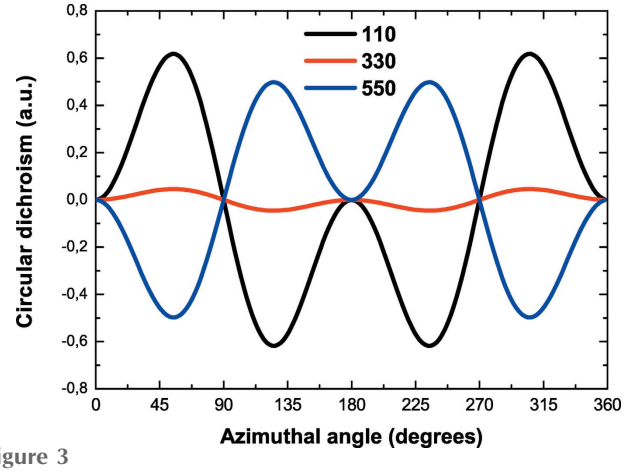

Figure 3
Azimuthal dependencies of circular dichroism for ($hh0$) forbidden reflections.

Table 1
Coefficients for various forbidden reflections.

Reflection	$\sin(4\pi hx)$	θ	$\Delta I_\pm(hh0)/\Delta I_\pm(110)$
110	0.8543	4.869	1
330	0.0691	14.752	0.074
550	−0.9177	25.112	−0.806

The largest dichroic signal is expected for the 110 and 550 reflections, whereas it is more than one order of magnitude weaker for the 330 reflection.

3. Experimental

The resonant X-ray scattering experiments were performed at ESRF beamline ID12 which offers full control of the polarization state of incident X-rays in the photon energy range from 2 to 15 keV. For the experiments at the Cu K-edge (∼9 keV) we used the second harmonic of radiation emitted by a helical undulator of Helios-II type with magnetic period of 52 mm. A fixed-exit monochromator was equipped with a pair of Si ⟨111⟩ crystals diffracting in the vertical plane. The crystals were cooled down to 140 K by refrigerated helium gas. The degree of circular polarization of the monochromatic X-rays was estimated to be more than 0.95. Higher-order harmonics of the undulator emission on axis in pure helical mode were well below the detection limit and therefore the use of mirrors was not necessary. The experiments were performed using an X-ray scattering end-station, shown in Figure 4. It is essentially a high-vacuum three-circle diffractometer operating in horizontal scattering geometry with a sample and detector arm rotations driven from outside the vacuum by Huber goniometers with a very high accuracy and an excellent reproducibility of 5 µrad.

The sample holder (or eventually a cold finger of a cryostat) is mounted on the axis of a goniometer allowing rotation of a crystal around the scattering vector (azimuthal scan). The

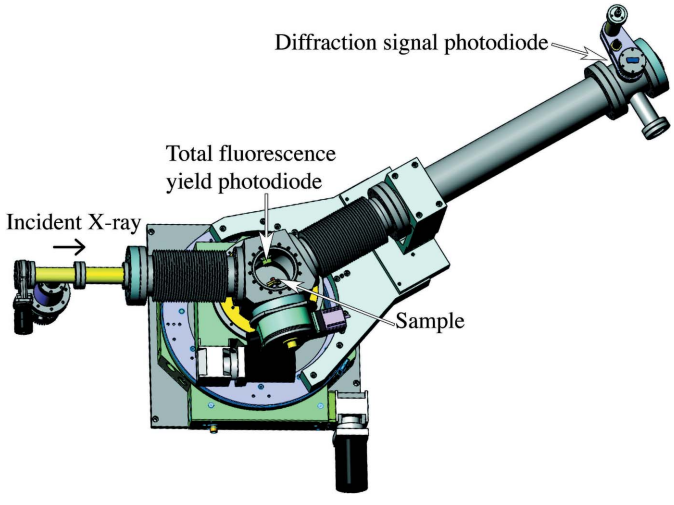

Figure 4
Schematic representation of the high-vacuum three-axis diffractometer at ESRF beamline ID12 equipped with a chamber allowing the θ angular range 12–48° to be covered.

diffractometer is connected to the beamline using flexible bellows of diameter 100 mm so that the angular range of the θ scans are $\pm 18^\circ$. There are three interchangeable chambers covering the θ angular ranges from $0^\circ \pm 18^\circ$, 12°–48° and 27°–63°, respectively. We paid special attention to keep the rotation axis of the chamber (θ axis) to be strictly perpendicular to the beam direction and to coincide with the sample surface. A peculiar feature of this diffractometer is the possibility to record *simultaneously* the intensity of the diffracted beam and the total fluorescence yield using two independent Si photodiodes. The first one behind the slits with its width adjustable from 50 µm to 2 mm is mounted on a 1 m-long detection arm and measures the diffracted beam; the second photodiode collecting the fluorescence photons is located inside the chamber at ~4 cm from the sample (see Figure 4). Note that there is no window between the monochromator, the sample and the detectors which avoids the generation of the parasitic scattered X-rays. This is very important whenever detection of the weak signals is concerned, *e.g.* dichroism and/or forbidden reflections. Excellent signal-to-noise ratio in both detection channels is achieved exploiting a digital lock-in detection based on a square wave modulation of the incident X-ray beam at *ca.* 67 Hz using a mechanical chopper. Dark current and any low-frequency instabilities of the X-ray beam are efficiently eliminated. Moreover, being installed upstream with respect to the monochromator the chopper reduces the heat load on the first crystal by a factor of two and makes the whole set-up more stable.

High-quality single crystals of copper metaborate were grown by the Kyropulos method from the melt of oxides B_2O_3, CuO, Li_2O and MoO_3 (Aleksandrov *et al.*, 2003). A plane-parallel plate of (110) orientation with a size of 10 mm × 10 mm × 0.5 mm was cut from an X-ray oriented single-crystal and its surface was polished.

The diffracted intensity is measured as the integral over the rocking curve for a given reflection. We have recorded the intensities of the forbidden 330 and 110 reflections as a function of the photon energies in the vicinity of the Cu *K*-edge or at a fixed energy as a function of azimuthal angle. Circular dichroism signal was obtained as a direct difference of the diffracted intensities measured with left- and right-circular polarized incident X-rays. In the present experiments the total diffracted intensities were measured without any polarization analysis.

4. Results and discussion

In this section we present the results of circular dichroism in X-ray resonant scattering for the 110 and 330 reflections measured at the Cu *K*-edge which are complemented with quantum mechanical calculations using the *FDMNES* code (Joly, 2001; see also http://fdmnes.neel.cnrs.fr). We have measured the series of the rocking curves for the 330 and 110 reflections for the right- and left-circularly polarized incident X-rays across the absorption edge. Integration over the rocking curves gives the integrated intensity. The polarization averaged integrated intensities $I(hh0)_{\rm av}$ and the circular dichroism $\Delta I(h00)_{\pm}$ for both reflections were calculated using the results of two measurements for right- and left-polarized beam. They are shown in Figure 5 as a function of photon energy. The X-ray absorption spectrum at the Cu *K*-edge measured using total fluorescence yield detection mode is also reproduced in the figure. As one can see, both ⟨110⟩ and ⟨330⟩ forbidden reflections show very similar energy dependence with two maxima at ~8991 eV and ~8998 eV corresponding to dipolar $1s \rightarrow 4p$ transitions in copper atoms. A small peak centered at 8981.5 eV in the absorption spectrum and $I(hh0)_{\rm av}(E)$ is due to $1s \rightarrow nd$ scattering events, but it is absent in the $\Delta I(h00)_{\pm}(E)$ spectrum. The polarization-averaged intensity of the 330 reflection was found, however, to be nearly three times stronger than that of the 110 reflection, which is in good agreement with theoretical predictions (see Section 2.1). On the other hand, the circular dichroism for the ⟨330⟩ reflection measured at the same azimuthal angle is found to be more than 20 times weaker than for the ⟨110⟩ reflection. The latter circular dichroism signal is surprisingly high and is comparable with the polarization averaged intensity of ⟨110⟩ diffracted intensities at the azimuthal angle $\phi = 30^\circ$.

The measurements of the 330 reflections were made at three different azimuthal angles revealing the maximum at about $\phi = 40^\circ$. The circular dichroism signal, *i.e.* the difference between the integrated intensities corresponding to the left- and right-circular polarizations of the incident beam, was observed for both reflections, but it was much stronger for the 110 reflection confirming the predictions based on symmetry considerations (see Section 2.1).

The energy spectra of the 330 and 110 reflections near the Cu *K*-edge was calculated using two methods realized in the *FDMNES* code: multiple scattering and the finite difference methods (FDM) taking into account the *E*1*E*1, *E*1.*E*2 and *E*2.*E*2 multipole contributions corresponding to both copper

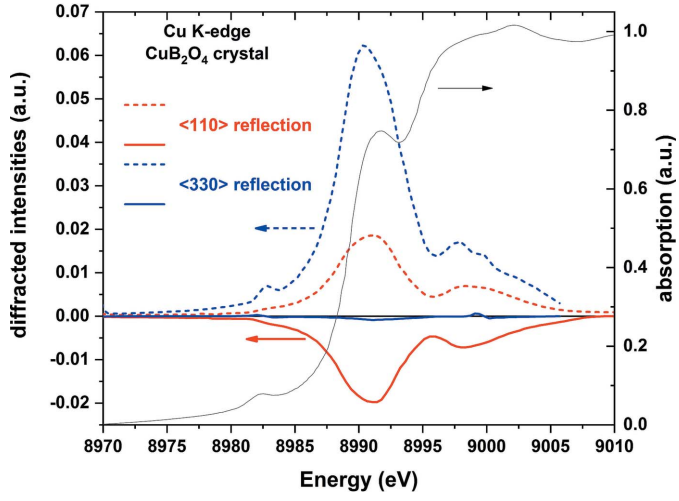

Figure 5
Experimental spectra of the polarization-averaged integrated intensities of the 110 (red lines) and 330 (blue lines) reflections (dotted lines) and corresponding circular dichroism (full lines) measured at the Cu *K*-edge at azimuthal angle $\phi = 30^\circ$. The total fluorescence yield detected Cu *K*-edge X-ray absorption spectrum (right-hand scale) of CuB_2O_4 single crystal is also shown.

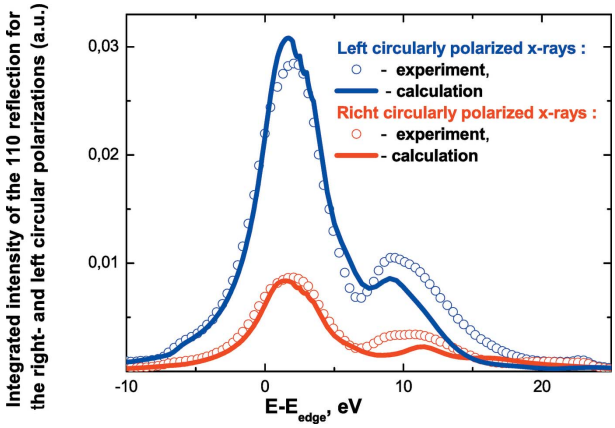

Figure 6
The energy spectrum of the 110 reflection for the right (red) and left (blue) circular polarizations (symbols: experiment; lines: calculation).

sites. In the multiple scattering option, all the atoms inside a sphere of radius 7.5 Å were involved in calculations while in the FDM method a radius equal to 5.8 Å gave satisfactory results. Some other parameters, for example the energy dependence of the full width of the excited state $\Gamma(E)$ and the shift between the spectra corresponding to the different copper positions, were taken from the previous studies of the absorption and XNCD in copper metaborate (Ovchinnikova *et al.*, 2016). Figure 6 demonstrates the calculated energy spectrum of the 110 reflection in comparison with the experimentally measured spectrum at the azimuthal angle $\phi = 45^\circ$. The calculations of the *hh*0 reflections energy spectra have shown that the $E1.E1$ contribution to the resonant scattering close to the Cu *K*-edge is predominant, which shows the fairness of the approach described above and the adequacy of the expressions describing the polarization properties of these reflections.

Azimuthal dependencies of the 110 reflection $I_+(100)$ and $I_-(100)$ measured with right- and left-polarizations of the incident radiation are shown in Figure 7 together with the fit using the expression (28) given in Section 2.1. The azimuthal dependencies of the 100 reflection average intensity and of its circular dichroism are shown in Figure 8 together with calculations based on the use of the expressions (27) and (28). In calculations the values $|f_{yz}|$ and $|f_{xx} - f_{yy}|$ are supposed to be variable parameters.

We see that the circular dichroism changes its sign at $\phi = 0^\circ$ and $\phi = 180^\circ$. At those angles the wavevectors **k** and **k**′ lie in the mirror plane close to the *z*-axis (the Bragg angle for the 110 reflection is small, 4.88°). At the angles $\phi = 90^\circ$ and $\phi = 270^\circ$ the wavevectors lie in the plane **ab** close to the fourfold axis, and the circular dichroism does not change its sign.

It follows from expression (27) that it is possible to determine the value $|f_{yz}|/|f_{xx} - f_{yy}|$ just from the experimental data as follows,

$$|f_{yz}|/|f_{xx} - f_{yy}| = \cot\theta \tan(2\pi hx)\left[\frac{I(\phi = 0)}{I(\phi = \pi/2) - I(\phi = 0)}\right]^{1/2}. \quad (29)$$

The substitution of the experimental data with the values given in Table 1 gives the value $|f_{yz}|/|f_{xx} - f_{yy}| = 0.572$.

Equation (28) can be rewritten as follows,

$$\Delta I_{\pm}(hh0) = 2\sqrt{2}\sin\phi\sin(2\phi)\cos^3\theta\sin(4\pi hx) \times |f_{yz}||f_{xx} - f_{yy}|\cos(\Delta\alpha), \quad (30)$$

where $\Delta\alpha$ is a relative phase describing tensor components: $\Delta\alpha = \alpha_{xx,yy} - \alpha_{yz}$, $\tan\alpha_{xx,yy} = (\mathrm{Im}\,f_{xx} - \mathrm{Im}\,f_{yy})/(\mathrm{Re}\,f_{xx} - \mathrm{Re}\,f_{yy})$, $\tan\alpha_{yz} = (\mathrm{Im}\,f_{yz}/\mathrm{Re}\,f_{yz})$, and $\mathrm{Re}f$ and $\mathrm{Im}f$ are the real and imaginary parts of the complex tensor components.

This relative phase can be calculated using the experimental data for the 110 reflection. It is equal to

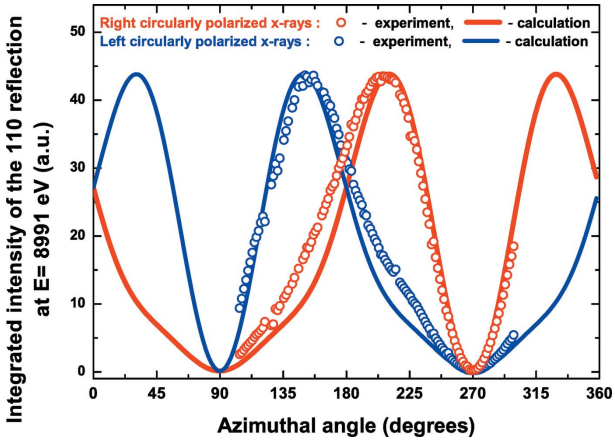

Figure 7
Azimuthal dependencies of the 110 reflection $I_+(100)$ (red) and $I_-(100)$ (blue) measured with right- and left-polarizations of the incident radiation at the energy 8991 eV.

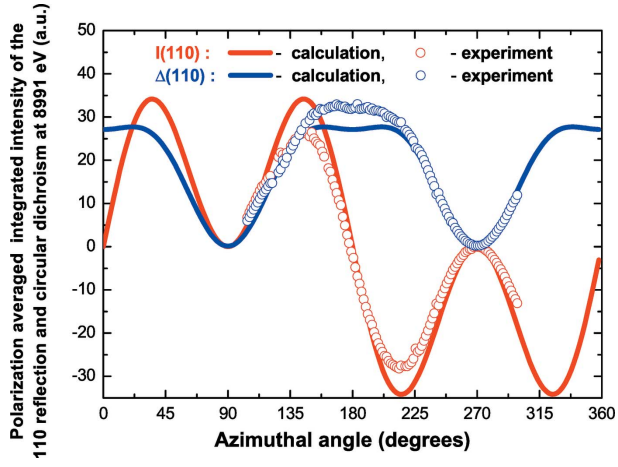

Figure 8
Azimuthal dependence of the polarization-averaged integrated intensity $I(110)_{av}$ (blue) and circular dichroism $\Delta I(110)_{\pm}$ (red) at the energy 8991 eV.

$$\cos(\Delta\alpha) = \frac{\sin\theta\,\Delta I(\phi=\pi/4)}{2\cos^2\theta\left\{I(\phi=0)[I(\phi=\pi/2)-I(\phi=0)]\right\}^{1/2}}. \quad (31)$$

Substitution of the experimental data into equation (31) gives $\Delta\alpha = 78^\circ$.

Let us discuss the physical meaning of the obtained quantities. The dipole–dipole atomic factor is a tensor of the second rank, which can be reduced to the system of principal axes that characterize the crystal field at the location of the Cu(B) atoms. In this system of principal axes, the tensor is diagonal. In the crystal field, p electronic states split into three sublevels usually described as p_x, p_y and p_z orbitals, where x, y and z are the main axes of the local anisotropy. In the considered case, the x-axis of the second rank tensor f_{ij} at the Cu(B1) atom coincides with the **a** crystal axis, but the main axes y and z do not coincide with crystal axes **b** and **c**. The axes of local anisotropy can be aligned with the axes of the crystal by rotation around the **a** axis by an angle equal to $\delta = (1/2)\arctan[f_{yz}/(f_{zz}-f_{xx})]$. Unfortunately, some additional information about the tensor components f_{xx} or f_{zz} is necessary to determine the absolute value of δ for the Cu(B) site in copper metaborate. Usually only the relative values can be determined from the experimental data. Absolute values of f_{ij} can be obtained only in comparison with the known value as shown by Mukhamedzhanov *et al.* (2007).

Taking into account that $f_{yz} = (f_{zz}-f_{xx})\tan 2\delta$, it also follows from equation (30) that $f_{xx} \neq f_{yy}$ and $f_{zz} \neq f_{yy}$, hence all p electron states at the Cu(B) site are split. Each diagonal tensor component describes resonant scattering through a certain sublevel. Because D_{ij} in equation (13) for the $E1.E1$ scattering is a real function depending on energy, the imaginary parts of the tensor components appear exclusively due to the resonant denominator in (12). So, the phases corresponding to all tensor components f_{ii} are equal to

$$\alpha_{ii} = \arctan\frac{\mathrm{Im}(f_{ii})}{\mathrm{Re}(f|_{ii})} = \arctan\frac{\Gamma}{2\left[\hbar\omega-\left(E_f-E_g\right)\right]}. \quad (32)$$

If the excited electronic levels are degenerate, then the energies E_f are the same for all electronic transitions, hence α_{ii} is the same for all tensor components, $\Delta\alpha_{ii}=0$. However, there is no circular dichroism in this case, because the diagonal tensor components are equal to each other. When the excited states split in a crystal field, α_{ii} may be different providing a phase shift between the tensor components. So, both the value obtained from equation (29) and the value from equation (31) characterize the degree of the levels splitting. However, we need more information to draw more specific conclusions about the tensor components f_{ij} corresponding to the Cu(B) sites. Those data could be obtained, for example, from the study of circular dichroism of other reflections, including allowed reflections. However, in copper metaborate both copper sites contribute to the allowed reflections which strongly complicates the interpretation of the data.

5. Conclusions

We have proposed and experimentally realized a new method based on measurements of the circular dichroism of Bragg reflections. It differs from XNCD in absorption because it is caused not only by the mixed $E1.E2$ multipoles but also by other kinds of multipoles, even by $E1.E1$, and therefore the dichroism can be very strong. However, similarly to XNCD, circular dichroism in Bragg diffraction can exist only in crystals without an inversion center. The great advantage of this method is that it allows to study separately resonant scattering by different Wyckoff sites, while all atoms together contribute to absorption and XNCD. This was demonstrated in a study of the 330 and 110 forbidden reflections in copper metaborate carried out at beamline ID12 of the ESRF. These forbidden reflections at incident radiation energies close the Cu K-edge exist exclusively due to Cu(B) atomic sites. The measurements of the XNCD signal in copper metaborate (Ovchinnikova *et al.*, 2016) have shown that it exists at almost the same energies as circular dichroism of the 330 and 110 reflections observed in the present study, but both copper sites contribute to the XNCD. It means that in the vicinity of the Cu K-edge there are many kinds of various electronic states, which may provide the interference between the waves in various multipole transitions, which can be revealed due to the various kinds of circular dichroism. However, the contributions of higher-order multipoles is negligible for the $hh0$ reflections in copper metaborate, so their energy and azimuthal dependencies are well described by only the $E1.E1$ transition.

In this paper we show that use of circularly polarized radiation in Bragg diffraction is useful not only to study chirality of matter, as carried out by Tanaka *et al.* (2008) and Usui *et al.* (2014), but being further developed it will allow us to obtain some quantitative physical information about splitting of electronic states in crystals. The proposed method may be realized not only for forbidden reflections but also for allowed reflections. However, in the latter case, it needs very high quality circularly polarized beams because even a small amount of linear polarization can essentially spoil the results. Further development of the method requires consideration of other reflections, higher-order transitions, taking into account the magnetic contribution to the scattering amplitude, as well as interference of different scattering channels.

Funding information

Work was partly supported by the Ministry of Science and Higher Education of the Russian Federation (state task for the Federal Research Center Crystallography and Photonics, Russian Academy of Sciences). This work was supported by the Russian Foundation for Basic Research (project No. 19-52-12029, study of the forbidden Bragg reflections, and project No. 19-02-00483, study of the use of circular polarization and the effect of Renninger reflections).

References

Alagna, L., Prosperi, T., Turchini, S., Goulon, J., Rogalev, A., Goulon-Ginet, C., Natoli, C. R., Peacock, R. D. & Stewart, B. (1998). *Phys. Rev. Lett.* **80**, 4799–4802.

Aleksandrov, K. S., Sorokin, B. P., Glushkov, D. A., Bezmaternykh, L. N., Burkov, S. I. & Belushchenko, S. V. (2003). *Phys. Solid State*, **45**, 42–45.

Arima, T. & Saito, M. (2009). *J. Phys. Condens. Matter*, **21**, 498001.

Barron, L. D. (1982). *Molecular Light Scattering and Optical Activity*. Cambridge University Press.

Belyakov, V. A. & Dmitrienko, V. E. (1989). *Sov. Phys. Usp.* **32**, 697–719.

Beutier, G., Collins, S. P., Nisbet, G., Akimova, K. A., Ovchinnikova, E. N., Oreshko, A. P. & Dmitrienko, V. E. (2015). *Phys. Rev. B*, **92**, 214116.

Beutier, G., Collins, S. P., Ovchinnikova, E. N., Nisbet, G. & Dmitrienko, V. E. (2014). *J. Phys. Conf. Ser.* **519**, 012006.

Blume, M. (1994). *Resonant Anomalous X-ray Scattering*, edited by G. Materlik, C. J. Spark & K. Fisher, pp. 495–515. Amsterdam: North-Holland.

Boehm, M., Roessli, B., Schefer, J., Wills, A. S., Ouladdiaf, B., Lelièvre-Berna, E., Staub, U. & Petrakovskii, G. A. (2003). *Phys. Rev. B*, **68**, 024405.

Boldyrev, K. N., Pisarev, R. V., Bezmaternykh, L. N. & Popova, M. N. (2015). *Phys. Rev. Lett.* **114**, 247210.

Brouder, C. (1990). *J. Phys. Condens. Matter*, **2**, 701–738.

Buckingham, A. D. (1967). *Adv. Chem. Phys.* **12**, 107–142.

Carra, P. & Benoist, R. (2000). *Phys. Rev. B*, **62**, R7703–R7706.

Carra, P., Jerez, A. & Marri, I. (2003). *Phys. Rev. B*, **67**, 045111.

Carra, P. & Thole, B. T. (1994). *Rev. Mod. Phys.* **66**, 1509–1515.

Collins, S. P., Laundy, D., Dmitrienko, V. E., Mannix, D. & Thompson, P. (2003). *Phys. Rev. B*, **68**, 064110.

Collins, S. P., Lovesey, S. W. & Balcar, E. (2007). *J. Phys. Condens. Matter*, **19**, 213201.

Dmitrienko, V. E. (1983). *Acta Cryst.* A**39**, 29–35.

Dmitrienko, V. E. (1984). *Acta Cryst.* A**40**, 89–95.

Dmitrienko, V. E., Ishida, K., Kirfel, A. & Ovchinnikova, E. N. (2005). *Acta Cryst.* A**61**, 481–493.

Dmitrienko, V. E., Kirfel, A. & Ovchinnikova, E. N. (2013). *International Tables for Crystallography*, Vol. D, ch 1.1, pp. 269–283. Dordrecht: Kluwer Academic Publishers.

Dmitrienko, V. E. & Ovchinnikova, E. N. (2000). *Acta Cryst.* A**56**, 340–347.

Dmitrienko, V. E. & Ovchinnikova, E. N. (2001). *Acta Cryst.* A**57**, 642–648.

Dmitrienko, V. E. & Ovchinnikova, E. N. (2003). *Crystallogr. Rep.* **48**, S52–S68. Translated from *Kristallografiya* **48**, S59–S77.

Dmitrienko, V. E., Ovchinnikova, E. N., Collins, S. P., Nisbet, G., Beutier, G., Kvashnin, Y. O., Mazurenko, V. G., Lichtenstein, A. I. & Katsnelson, M. I. (2014). *Nat. Phys.* **10**, 202–206.

Dmitrienko, V. E., Ovchinnikova, E. N. & Ishida, K. (1999). *JETP Lett.* **69**, 938–942.

Dmitrienko, V. E., Ovchinnikova, E. N., Kokubun, J. & Ishida, K. (2010). *JETP Lett.* **92**, 383–387.

Fiebig, M., Sänger, I. & Pisarev, R. V. (2003). *J. Appl. Phys.* **93**, 6960–6962.

Finkelstein, K. D., Hamrick, M. & Shen, Q. (1994). *Resonant Anomalous X-ray Scattering*, edited by G. Materlik, C. J. Spark & K. Fisher, pp. 91–97. Amsterdam: North-Holland.

Finkelstein, K. D., Shen, Q. & Shastri, S. (1992). *Phys. Rev. Lett.* **69**, 1612–1615.

Goulon, J., Goulon-Ginet, C., Rogalev, A., Gotte, V., Malgrange, C. & Brouder, C. (1999). *J. Synchrotron Rad.* **6**, 673–675.

Goulon, J., Goulon-Ginet, C., Rogalev, A., Gotte, V., Malgrange, C., Brouder, Ch. & Natoli, C. R. (1998). *J. Chem. Phys.* **108**, 6394–6403.

Goulon, J., Jaouen, N., Rogalev, A., Wilhelm, F., Goulon-Ginet, Ch., Brouder, Ch., Joly, Y., Ovchinnikova, E. N. & Dmitrienko, V. E. (2007). *J. Phys. Condens. Matter*, **19**, 156201–156219.

Goulon, J., Rogalev, A., Wilhelm, F., Goulon-Ginet, C., Carra, P., Marri, I. & Brouder, Ch. (2003). *J. Exp. Theor. Phys.* **97**, 402–431.

Hahn, Th. (1996). Editor. *International Tables for Crystallography*, Vol. A. Dordrecht: Kluwer Academic Publishers.

Hannon, J. P., Trammell, G. T., Blume, M. & Gibbs, D. (1988). *Phys. Rev. Lett.* **61**, 1245–1248.

Izumi, Y., Tanabe, M., Imazu, A., Mimoto, A., Tanaka, M., Agui, A., Muro, T. & Nakagawa, K. (2013). *J. Chem. Phys.* **138**, 074305.

James, R. W. (1950). *The Optical Principles of the Diffraction of X-rays*. London: G. Bell and Sons.

Jerphagnon, J. & Chemla, D. S. (1976). *J. Chem. Phys.* **65**, 1522–1529.

Jerphagnon, J., Chemla, D. S. & Bonneville, R. (1978). *Adv. Phys.* **27**, 609–650.

Joly, Y. (2001). *Phys. Rev. B*, **63**, 125120.

Khanh, N. D., Abe, N., Kubo, K., Akaki, M., Tokunaga, M., Sasaki, T. & Arima, T. (2013). *Phys. Rev. B*, **87**, 184416.

Kirfel, A., Grybos, J. & Dmitrienko, V. E. (2002). *Phys. Rev. B*, **66**, 165202.

Kokubun, J., Kanazawa, M., Ishida, K. & Dmitrienko, V. E. (2001). *Phys. Rev. B*, **64**, 073203.

Lovesey, S. W. (2016). *Phys. Rev. B*, **94**, 094422.

Lovesey, S. W., Balcar, E., Knight, K. S. & Fernandezrodriguez, J. (2005). *Phys. Rep.* **411**, 233–289.

Lovesey, S. W. & Collins, S. P. (1996). *X-ray Scattering and Absorption by Magnetic Materials*. Oxford Science Publications.

Lovesey, S. W. & Staub, U. (2009). *J. Phys. Condens. Matter*, **21**, 142201.

Martinez-Ripoll, M., Martínez-Carrera, S. & García-Blanco, S. (1971). *Acta Cryst.* B**27**, 677–681.

Matteo, S. D., Joly, Y., Bombardi, A., Paolasini, L., de Bergevin, F. & Natoli, C. (2003). *Phys. Rev. Lett.* **91**, 257402.

Mero, R. D., Lai, C.-H., Du, C.-H. & Liu, H.-L. (2021). *J. Phys. Chem. C*, **125**, 4322–4329.

Mukhamedzhanov, E. Kh., Borisov, M. M., Morkovin, A. N., Antonenko, A. A., Oreshko, A. P., Ovchinnikova, E. N. & Dmitrienko, V. E. (2007). *JETP Lett.* **86**, 783–787.

Natoli, C. R., Brouder, Ch., Sainctavit, Ph., Goulon, J., Goulon-Ginet, C. & Rogalev, A. (1998). *Eur. Phys. J. B*, **4**, 1–11.

Nénert, G., Bezmaternykh, L. N., Vasiliev, A. N. & Palstra, T. T. M. (2007). *Phys. Rev. B*, **76**, 144401.

Oreshko, A. P., Ovchinnikova, E. N., Beutier, G., Collins, S. P., Nisbet, G., Kolchinskaya, A. M. & Dmitrienko, V. E. (2012). *J. Phys. Condens. Matter*, **24**, 245403.

Ovchinnikova, E. N., Dmitrienko, V. E., Kozlovskaya, K. A. & Rogalev, A. (2019). *JETP Lett.* **110**, 568–573.

Ovchinnikova, E. N., Rogalev, A., Wilhelm, F., Kozlovskaya, K. A., Oreshko, A. P. & Dmitrienko, V. E. (2016). *J. Exp. Theor. Phys.* **123**, 27–32.

Peacock, R. D. & Stewart, B. (2001). *J. Phys. Chem. B*, **105**, 351–360.

Petrakovskii, G., Velikanov, D., Vorotinov, A., Balaev, A., Sablina, K., Amato, A., Roessli, B., Schefer, J. & Staub, U. (1999). *J. Magn. Magn. Mater.* **205**, 105–109.

Pisarev, R. V., Sänger, I., Petrakovskii, G. A. & Fiebig, M. (2004). *Phys. Rev. Lett.* **93**, 037204.

Platunov, M., Gudim, I., Ovchinnikova, E., Kozlovskaya, K., Wilhelm, F., Rogalev, A., Hen, F., Ivanov, V. Yu., Mukhin, A. & Dmitrienko, V. E. (2021). *Crystals*, **11**, 531–544.

Richter, C., Novikov, D. V., Mukhamedzhanov, E. Kh., Borisov, M. M., Akimova, K. A., Ovchinnikova, E. N., Oreshko, A. P., Strempfer, J., Zschornak, M., Mehner, E., Meyer, D. C. & Dmitrienko, V. E. (2014). *Phys. Rev. B*, **89**, 094110.

Saito, M., Ishikawa, K., Taniguchi, K. & Arima, T. (2008*a*). *Phys. Rev. Lett.* **101**, 117402.

Saito, M., Taniguchi, K. & Arima, T. (2008*b*). *J. Phys. Soc. Jpn*, **77**, 013705.

Sirotine, Yu. & Chaskolskaia, M. P. (1982). *Fundamentals of Crystal Physics.* Moscow: Mir.
Tanaka, Y., Collins, S. P., Lovesey, S. W., Matsumami, M., Moriwaki, T. & Shin, S. (2010). *J. Phys. Condens. Matter*, **22**, 122201.
Tanaka, Y., Takeuchi, T., Lovesey, S. W., Knight, K. S., Chainani, A., Takata, Y., Oura, M., Senba, Y., Ohashi, H. & Shin, S. (2008). *Phys. Rev. Lett.* **100**, 145502.
Templeton, D. H. & Templeton, L. K. (1985*a*). *Acta Cryst.* A**41**, 133–142.
Templeton, D. H. & Templeton, L. K. (1985*b*). *Acta Cryst.* A**41**, 365–371.
Templeton, D. H. & Templeton, L. K. (1986). *Acta Cryst.* A**42**, 478–481.
Templeton, D. H. & Templeton, L. K. (1994). *Phys. Rev. B*, **49**, 14850–14853.
Usui, T., Tanaka, Y., Nakajima, H., Taguchi, M., Chainani, A., Oura, M., Shin, S., Katayama, N., Sawa, H., Wakabayashi, Y. & Kimura, T. (2014). *Nat. Mater.* **13**, 611–618.